Research Article | Vol. 25, No. 3 | 6 Feb 2017 | OPTICS EXPRESS 1958

Optics EXPRESS

Using X-ray spectroscopy of relativistic laser plasma interaction to reveal parametric decay instabilities: a modeling tool for astrophysics

E. OKS,[1,12] E. DALIMIER,[2] A.YA. FAENOV,[3,4,13] P. ANGELO,[2] S.A. PIKUZ,[4,5] E. TUBMAN,[6] N.M.H. BUTLER,[7] R.J. DANCE,[7] T.A. PIKUZ,[4,8] I.YU. SKOBELEV,[4,5] M.A. ALKHIMOVA,[4,5] N. BOOTH,[9] J. GREEN,[9] C. GREGORY,[9] A. ANDREEV,[10,11] A. ZHIDKOV,[8] R. KODAMA,[3,8] P. MCKENNA,[7] AND N. WOOLSEY[6]

[1]*Physics Department, 206 Allison Lab, Auburn University, AL 36849, USA*
[2]*LULI - UPMC Univ Paris 06: Sorbonne Universités ; CNRS, Ecole Polytechnique, CEA: Université Paris-Saclay - F-75252 Paris cedex 05, France*
[3]*Institute for Academic Initiatives, Osaka University, Suita, Osaka, 565-0871, Japan*
[4]*Joint Institute for High Temperatures, Russian Academy of Sciences, Moscow 125412, Russia*
[5]*National Research Nuclear University MEPhI, Moscow 115409, Russia.*
[6]*York Plasma Institute, Department of Physics, University of York, York YO10 5DD, UK*
[7]*Department of Physics, SUPA, University of Strathclyde, Glasgow G4 0NG, UK*
[8]*PPC and Graduate School of Engineering, Osaka University, 2-1, Yamadaoka, Suita, Osaka 565-0871, Japan*
[9]*Central Laser Facility, STFC Rutherford Appleton Laboratory, Didcot OX11 0QX, UK*
[10]*Max Born Institute, Berlin 12489, Max-Born str. 2a, Berlin, Germany*
[11]*ELI-ALPS, Szeged H-6720, Hungary*
[12]*goks@physics.auburn.edu*
[13]*faenov.anatoly@photon.osaka-u.ac.jp*

Abstract: By analyzing profiles of experimental x-ray spectral lines of Si XIV and Al XIII, we found that both Langmuir and ion acoustic waves developed in plasmas produced via irradiation of thin Si foils by relativistic laser pulses (intensities ~10^{21} W/cm^2). We prove that these waves are due to the parametric decay instability (PDI). This is the first time that the PDI-induced ion acoustic turbulence was discovered by the x-ray spectroscopy in laser-produced plasmas. These conclusions are also supported by PIC simulations. Our results can be used for laboratory modeling of physical processes in astrophysical objects and a better understanding of intense laser-plasma interactions.

OCIS codes: (020.2649) Strong field laser physics; (320.2250) Femtosecond phenomena; (300.6560) Spectroscopy, x-ray; (350.5400) Plasmas; (020.3690) Line shapes and shifts; (350.1270) Astronomy and astrophysics

References and links

1. V. N. Tsytovich, *Theory of Turbulent Plasmas (*Springer, 1977).
2. B. B. Kadomtsev, *Plasma Turbulence (*Academic, 1965).
3. W. Ebeling, *Transport Properties of Dense Plasmas* (Birkhäuser, 1984).
4. G. Manfredi and R. O. Dendy, "Transport properties of energetic particles in a turbulent electrostatic field," Phys. Plasmas **4**(3), 628–635 (1997).
5. A. I. Zhuzhunashvili and E. Oks, "Technique of optical polarization measurements of the plasma Langmuir turbulence spectrum," Sov. Phys. JETP **46**, 1122–1132 (1977).
6. E. Oks and V. A. Rantsev-Kartinov, "Spectroscopic observation and analysis of plasma turbulence in a Z-pinch," Sov. Phys. JETP **52**, 50–58 (1980).
7. L. Jian, X. Shali, Y. Qingguo, L. Lifeng, and W. Yufen, "Spatially-resolved spectra from a new uniform dispersion crystal spectrometer for characterization of Z-pinch plasmas," J. Quant. Spectrosc. Radiat. Transf. **116**, 41–48 (2013).
8. E. A. Oks, S. Böddeker, and H. Kunze, "Spectroscopy of atomic hydrogen in dense plasmas in the presence of dynamic fields: Intra-Stark spectroscopy," Phys. Rev. A **44**(12), 8338–8347 (1991).

#276415 http://dx.doi.org/10.1364/OE.25.001958
Journal © 2017 Received 3 Oct 2016; revised 8 Jan 2017; accepted 9 Jan 2017; published 24 Jan 2017
Corrected: 25 January 2017

Optics EXPRESS

9. E. Oks, *Plasma Spectroscopy: The Influence of Microwave and Laser Fields, Springer Series on Atoms and Plasmas*, vol. 9 (Springer, 1995).
10. A. S. Antonov, O. A. Zinov'ev, V. D. Rusanov, and A. V. Titov, "Broadening of hydrogen spectral lines during turbulent heating of a plasma," Sov. Phys. JETP **31**, 838–839 (1970).
11. S. P. Zagorodnikov, G. E. Smolkin, E. A. Striganova, and G. V. Sholin, "Method of measurement of nonequilibrium electric fields in a turbulent plasma from Stark broadening of the spectral lines of hydrogen," Sov. Phys. Dokl. **15**, 1122–1125 (1971).
12. E. K. Zavojskij, J. G. Kalinin, V. A. Skorjupin, V. V. Shapkin, and G. V. Sholin, "Measurement of electric fields in a turbulent plasma by the Stark broadening of the spectral lines of hydrogen," Sov. Phys. Dokl. **15**, 823–826 (1971).
13. M. A. Levine and C. C. Gallagher, "Stark broadening for turbulence studies in a confined plasma," Phys. Lett. A **32**(1), 14–15 (1970).
14. N. Ben-Yosef and A. G. Rubin, "Optical investigations of electrostatic turbulence in plasma," Phys. Lett. A **33**(4), 222–223 (1970).
15. A. B. Berezin, A. V. Dubovoj, and B. V. Ljublin, "Anisotropic electric fields due to ion-acoustic turbulence in a rf discharge," Sov. Phys. Tech. Phys. **16**, 1844–1846 (1972).
16. M. V. Babykin, A. I. Zhuzhunashvili, E. Oks, V. V. Shapkin, and G. V. Sholin, "Polarization spectroscopic analysis of noise produced in a turbulent plasma upon annihilation of oppositely moving magnetic fields," Sov. Phys. JETP **38**, 86–92 (1974).
17. J. F. Volkov, V. G. Djatlov, and A. I. Mitina, "Optical investigation of a turbulent plasma," Sov. Phys. Tech. Phys. **19**, 905–908 (1975).
18. A. B. Berezin, B. V. Ljublin, and D. G. Jakovlev, "Study of plasma turbulence in a fast linear theta-pinch by means of Stark broadening of deuterium spectral lines," Sov. Phys. Tech. Phys. **28**, 407–411 (1983).
19. A. N. Koval and E. Oks, "Some results of searching for low-frequency plasma turbulence in large chromospheric flares," Bull. Crimean Astrophys. Observatory **67**, 78–89 (1983).
20. A. G. Frank, V. P. Gavrilenko, N. P. Kyrie, and E. Oks, "Spectroscopic study of anomalous electric fields in peripheral regions of a current sheet plasma," J. Phys. At. Mol. Opt. Phys. **39**(24), 5119–5129 (2006).
21. A. Pukhov, "Strong field interaction of laser radiation," Rep. Prog. Phys. **66**(1), 47–101 (2003).
22. P. McKenna, D. Neely, R. Bingham, and D. Jaroszynski, *Laser-Plasma Interactions and Applications* (Springer, 2013).
23. O. Renner, E. Dalimier, E. Oks, F. Krasniqi, E. Dufour, R. Schott, and E. Förster, "Experimental evidence of Langmuir-wave caused features in spectral lines of laser-produced plasmas," J. Quant. Spectrosc. Radiat. Transf. **99**(1-3), 439–450 (2006).
24. V. Springel, S. D. M. White, A. Jenkins, C. S. Frenk, N. Yoshida, L. Gao, J. Navarro, R. Thacker, D. Croton, J. Helly, J. A. Peacock, S. Cole, P. Thomas, H. Couchman, A. Evrard, J. Colberg, and F. Pearce, "Simulations of the formation, evolution and clustering of galaxies and quasars," Nature **435**(7042), 629–636 (2005).
25. T. Di Matteo, V. Springel, and L. Hernquist, "Energy input from quasars regulates the growth and activity of black holes and their host galaxies," Nature **433**(7026), 604–607 (2005).
26. B. M. Peterson, *An Introduction to Active Galactic Nuclei (*Cambridge University Press, 1997).
27. D. A. Lorimer and M. Kramer, *Handbook of Pulsar Astronomy (*Cambridge University Press, 2004).
28. R. T. Gangadhara and V. Krishan, "*Absorption of Electromagnetic Waves in Astrophysical Plasmas*," in *Basic Plasma Processes on the Sun*, E.R. Priest, and V. Krishan, eds. (Springer, 1990).
29. A. G. Frank, "Dynamics of current sheets underlying flare-type events in magnetized plasmas," Phys. Uspekhi **53**(9), 941–947 (2010).
30. S. V. Bulanov, V. A. Dogiel, and A. G. Frank, "Solar flares and magnetic reconnection experiments," Phys. Scr. **29**(1), 66–67 (1984).
31. B. Dromey, S. Kar, C. Bellei, D. C. Carroll, R. J. Clarke, J. S. Green, S. Kneip, K. Markey, S. R. Nagel, P. T. Simpson, L. Willingale, P. McKenna, D. Neely, Z. Najmudin, K. Krushelnick, P. A. Norreys, and M. Zepf, "Bright multi-keV harmonic generation from relativistically oscillating plasma surfaces," Phys. Rev. Lett. **99**(8), 085001 (2007).
32. C. N. Danson, P. A. Brummitt, R. J. Clarke, J. L. Collier, B. Fell, A. J. Frackiewicz, S. Hancock, S. Hawkes, C. Hernandez-Gomez, P. Holligan, M. H. R. Hutchinson, A. Kidd, W. J. Lester, I. O. Musgrave, D. Neely, D. R. Neville, P. A. Norreys, D. A. Pepler, C. J. Reason, W. Shaikh, T. B. Winstone, R. W. W. Wyatt, and B. E. Wyborn, "Vulcan Petawatt—an ultra-high-intensity interaction facility," Nucl. Fusion **44**(12), 5239–5246 (2004).
33. I. Musgrave, W. Shaikh, M. Galimberti, A. Boyle, C. Hernandez-Gomez, K. Lancaster, and R. Heathcote, "Picosecond optical parametric chirped pulse amplifier as a preamplifier to generate high-energy seed pulses for contrast enhancement," Appl. Opt. **49**(33), 6558–6562 (2010).
34. A. Ya. Faenov, S. A. Pikuz, A. I. Erko, B. A. Bryunetkin, V. M. Dyakin, G. V. Ivanenkov, A. R. Mingaleev, T. A. Pikuz, V. M. Romanova, and T. A. Shelkovenko, "High-performance X-ray spectroscopic devices for plasma microsources investigations," Phys. Scr. **50**(4), 333–338 (1994).
35. J. Colgan, J. Abdallah, Jr., A. Ya. Faenov, S. A. Pikuz, E. Wagenaars, N. Booth, O. Culfa, R. J. Dance, R. G. Evans, R. J. Gray, T. Kaempfer, K. L. Lancaster, P. McKenna, A. L. Rossall, I. Yu. Skobelev, K. S. Schulze, I. Uschmann, A. G. Zhidkov, and N. C. Woolsey, "Exotic dense-matter states pumped by a relativistic laser plasma in the radiation-dominated regime," Phys. Rev. Lett. **110**(12), 125001 (2013).

Optics EXPRESS

36. S. A. Pikuz, A. Ya. Faenov, J. Colgan, R. J. Dance, J. Abdallah, E. Wagenaars, N. Booth, O. Culfa, R. G. Evans, R. J. Gray, T. Kaempfer, K. L. Lancaster, P. McKenna, A. L. Rossall, I. Yu. Skobelev, K. S. Schulze, I. Uschmann, A. G. Zhidkov, and N. C. Woolsey, "Measurement and simulations of hollow atom X-ray spectra of solid-density relativistic plasma created by high-contrast PW optical laser pulses," High Energy Density Phys. **9**(3), 560–567 (2013).
37. J. Colgan, A. Ya. Faenov, S. A. Pikuz, E. Tubman, N. M. H. Butler, J. Abdallah jr., R. J. Dance, T. A. Pikuz, I. Yu. Skobelev, M. A. Alkhimova, N. Booth, J. Green, C. Gregory, A. Andreev, R. Lötz, I. Uschmann, A. Zhidkov, R. Kodama, P. McKenna, and N. Woolsey,."Evidence of high-n hollow-ion emission from Si ions pumped by ultraintense x-rays from relativistic laser plasma," Europhys. Lett. **114,** 35001 (2016)55.
38. V. P. Gavrilenko and E. A. Oks, "New effect in the Stark spectroscopy of atomic hydrogen: dynamic resonance," Sov. Phys. JETP **53**, 1122–1127 (1981).
39. P. Maine, D. Strickland, P. Bado, M. Pessot, and G. Mourou, "Generation of ultrahigh peak power pulses by chirped pulse amplification," IEEE J. Quantum Electron. **24**(2), 398–403 (1988).
40. A. I. Akhiezer and R. V. Polovin, "Theory of wave motion of an electron plasma," Sov. Phys. JETP **3**, 696–705 (1956).
41. W. Lünow, "On the relativistic non-linear interaction of cold plasma with electro-magnetic waves," Plasma Phys. **10**(9), 879–897 (1968).
42. S. Guérin, P. Mora, J. C. Adam, A. Heron, and G. Laval, "Propagation of ultraintense laser pulses through overdense plasma layers," Phys. Plasmas **3**(7), 2693–2701 (1996).
43. R. J. Gray, D. C. Carroll, X. H. Yuan, C. M. Brenner, M. Burza, M. Coury, K. L. Lancaster, X. X. Lin, Y. T. Li, D. Neely, M. N. Quinn, O. Tresca, C.-G. Wahlström, and P. McKenna, "Laser pulse propagation and enhanced energy coupling to fast electrons in dense plasma gradients," New J. Phys. **16**(11), 113075 (2014).
44. J. Fuchs, J. C. Adam, F. Amiranoff, S. D. Baton, P. Gallant, L. Gremillet, A. Heron, J. C. Kieffer, G. Laval, G. Malka, J. L. Miquel, P. Mora, N. Pepin, and C. Rousseaux, "Transmission through highly overdense plasma slabs with a subpicosecond relativistic laser pulse," Phys. Rev. Lett. **80**(11), 2326–2329 (1998).
45. H. K. Chung, M. H. Chen, W. L. Morgan, Yu. Ralchenko, and R. W. Lee, "Generalized population kinetics and spectral model for rapid spectroscopic analysis for all elements," High Energy Density Phys. **1**(1), 3–12 (2005).
46. A. Pukhov and J. Meyer-ter-Vehn, "Laser hole boring into overdense plasma and relativistic electron currents for fast ignition of ICF targets," Phys. Rev. Lett. **79**(14), 2686–2689 (1997).
47. G. A. Mourou, T. Tajima, and S. V. Bulanov, "Optics in the relativistic regime," Rev. Mod. Phys. **78**(2), 309–371 (2006).
48. P. Sauvan, E. Dalimier, E. Oks, O. Renner, S. Weber, and C. Riconda, "Spectroscopic diagnostics of plasma interaction with an external oscillatory field," J. Phys. At. Mol. Opt. Phys. **42**(19), 195501 (2009).
49. P. Gibbon, *Short Pulse Laser Interaction with Matter* (Imperial College Press, 2003)
50. V. S. Lisitsa, "Stark broadening of hydrogen lines in plasmas," Sov. Phys. Usp. **122**(7), 449–495 (1977).
51. E. Oks and G. V. Sholin, "On Stark profiles of hydrogen lines in a plasma with low-frequency turbulence," Sov. Phys. Tech. Phys. **21**, 144–151 (1976).
52. E. Oks and E. Dalimier, "Toward diagnostic of ionic sound in laser-produced plasmas," Intern. Rev. Atom. Mol. Phys. **2**, 43–51 (2011).
53. C. A. Iglesias, H. E. DeWitt, J. L. Lebowitz, D. MacGowan, and W. B. Hubbard, "Low-frequency electric microfield distributions in plasmas," Phys. Rev. A Gen. Phys. **31**(3), 1698–1702 (1985).
54. D. I. Blochinzew, "Zur Theorie des Starkeffektes in Zeitveränderlichen Feld," Phys. Z. Sow. Union **4**, 501–515 (1933).
55. R. Lichters, J. Meyer-ter-Vehn, and A. Pukhov, "Short pulse laser harmonics from oscillating plasma surfaces driven at relativistic intensity," Phys. Plasmas **3**(9), 3425–3437 (1996).
56. W. L. Kruer, *The Physics of Laser Plasma Interactions* (Westview Press, 2003).

1. Introduction

Shapes of x-ray spectral lines emitted by laser-produced plasmas have is a standard tool for measuring the electron density and the temperature of plasmas. In our study the experimental spectral lines were Si XIV and Al XIII lines generated via the interaction of a super-intense (relativistic) laser radiation (of the intensity ~10^{21} W/cm^2) with thin Si foils. By analysis of these experimental spectra we discovered the ion acoustic turbulence in this laser-produced plasma, which is the first experimental discovery of the ion acoustic turbulence in laser-produced plasmas by means of the x-ray spectroscopy – to the best of our knowledge. We proved that the ion acoustic turbulence developed at critical density surface of the laser-plasma interaction as a result of the parametric decay instability (PDI). Below we put this in prospective.

PDI is a nonlinear process in which an electromagnetic wave decays into a Langmuir wave and an ion acoustic wave. The resulting waves constitute two types of the electrostatic plasma turbulence. Electrostatic turbulence frequently occurs in various kinds of laboratory

Optics EXPRESS

and astrophysical plasmas [1,2]. It is represented by oscillatory electric fields corresponding to collective degrees of freedom in plasmas – in distinction to the electron and ion microfields that correspond to individual degrees of freedom of charged particles.

High-frequency plasma turbulence, namely Langmuir waves, develops at the electron plasma frequency $\omega_{pe} = (4\pi e^2 N_e/m_e)^{1/2} = 5.64x10^4 N_e^{1/2}$, where N_e is the electron density. In the case of Low-frequency Electrostatic plasma Turbulence (LET), in the absence of a magnetic field, only ion-acoustic waves are generated (a.k.a. ionic sound waves). They have a broad spectrum at frequencies below or of the order of the ion plasma frequency $\omega_{pi} = (4\pi e^2 N_i Z^2/m_i)^{1/2} = 1.32\ x10^3 Z(N_i m_p/m_i)^{1/2}$, where N_i is the ion density, Z is the charge state; m_p and m_i are the proton and ion masses, respectively. CGS units are used in the above formulas.

The LET strongly affects transport phenomena in various plasmas [3,4]. Plasmas subject to LET frequently exhibit properties such as anomalous resistivity, which changes the behavior of such plasmas significantly. Langmuir waves were discovered experimentally upon analysis of the shapes of neutral hydrogen spectral lines in many reliable experiments at various plasma sources and electron densities $N_e \sim 10^{14} - 10^{18}$ cm^{-3}, namely in a theta-pinch [5], Z-pinches [6,7], and a gas-liner pinch [8] – via the phenomenon (presented below) of the Langmuir-wave-caused dips (L-dips) in spectral line profiles. The majority of experimental studies, together with theoretical studies of L-dips are summarized in [9].

A variety of LET (including ion-acoustic waves) were diagnosed by an 'anomalous' broadening of neutral hydrogen spectral lines in experiments involving plasmas with low electron densities ($N_e \sim 10^{14}$ - 10^{16} cm^{-3}). Different types of discharges were used over these experiments [10–18]. The LET was also diagnosed in solar flares by a detailed analysis of the shapes of the observed spectral lines of neutral hydrogen [19], as well as in experiment [20] for laboratory modeling of mechanisms of solar flares.

The electrostatic waves/turbulence, such as, e.g., Langmuir waves and ion acoustic waves, can also develop in dense plasmas. In particular, in the area of laser-plasma interactions, they have been studied theoretically by many authors, including in the relativistic laser interactions with solid targets (see, e.g., [21,22] and references therein).

In laser-produced, high-density plasmas, Langmuir waves were discovered experimentally [23] via the phenomenon of L-dips in spectral line profiles of Al XIII. By contrast, ion acoustic waves (or any other kind of a LET) in laser-produced, high-density plasmas were not discovered experimentally up to now.

Below after presenting this discovery, we show that the ratio of the energy density of the turbulent electric fields $E^2/(8\pi)$ to the thermal energy density of the plasma N_eT (where T is the plasma temperature)) is of the same order of magnitude as the corresponding ratio in different astrophysical objects: quasars, pulsars, and Seyfert galaxies. Therefore, these kind of laboratory experiments can serve as a tool to model the PDI in these astrophysical objects.

For clarity: quasars, Seyfert galaxies, and pulsars are extremely luminous, intriguing astrophysical objects being very different from each other. Quasars are the most energetic and distant members of a class of objects called active galactic nuclei. They are extremely luminous. A quasar is a compact region in the center of a massive galaxy surrounding a central supermassive black hole – see, e.g [24,25]. Seyfert galaxies are members of another group of active galaxies, along with quasars. They have quasar-like nuclei (very luminous, distant and bright sources of electromagnetic radiation) with very high surface brightness, but unlike quasars, their host galaxies are clearly detectable – see, e.g [26]. A pulsar is a highly magnetized, rotating neutron star that emits a beam of electromagnetic radiation. Neutron stars are very dense, and have short, regular rotational periods. This produces a very precise interval between pulses that range roughly from milliseconds to seconds for an individual pulsar – see, e.g [27].

These very different astrophysical objects have one thing in common: in their atmosphere, the conditions are satisfied for the Parametric Decay Instability (PDI), causing the anomalous absorption of the incident electromagnetic radiation – see, e.g [28].

Optics EXPRESS

The possibility to use the x-ray spectroscopy in laboratory laser-plasma interaction experiments as a tool to model the PDI in these astrophysical objects is based on the same principle (the similarity of dimensionless parameters) that was used in various modeling experiments at plasmas not produced by lasers. For example, this principle of modeling was used for decades for the successful modeling of mechanisms of solar flares by laboratory experiments – see, e.g., review [29] and references therein. While the dimensional parameters in the two objects differed by many orders of magnitude, the relevant dimensionless parameters were of the same order of magnitude – see, e.g [30].

2. Results

2.1 X-ray spectra measurements

The experiments were performed at Vulcan Petawatt (PW) facility at the Rutherford Appleton Laboratory [31,32], which provides a beam using optical parametric, chirped pulse amplification (OPCPA) technology with a central wavelength of 1054 nm and a pulse full-width-half-maximum (FWHM) duration, which could be varied from 500 up to 1500 fs. The OPCPA approach enables an amplified spontaneous emission (ASE) to peak-intensity contrast ratio exceeding $1{:}10^9$ several nanoseconds before the peak of the laser pulse [33]. The laser pulse was focused with an f/3 off-axis parabola. At the best focus approximately 30% of the energy (up to 290 J on the target in our experiments) was contained within an 7 μm (FWHM) diameter spot providing a maximum intensity of 1.4×10^{21} W/cm^2. The horizontally polarized laser beam was incident on target at 45° from the target surface normal, as shown schematically in Fig. 1(a).

High-resolution spectroscopy measurements were performed using a Focusing Spectrometer with Spatial Resolution (FSSR) [34–36]. The instrument was equipped with a spherically bent mica crystal with a lattice spacing $2d$ ~19.94 Å and a radius of curvature of R = 100 mm. The crystal was aligned to operate at m = 3 order of reflection to record K-shell emission Rydberg H-like spectral lines of multicharged Si XIV ions in 4.85 – 5.35 Å wavelength range. The FSSR spectral resolving power was approximately 3000. The spectrometer viewed the laser-irradiated rear surface of the target at an angle of 5° to the target surface normal (Fig. 1(a)). Target-to-crystal distance of 367 mm led to a demagnification factor of ~4.7 for the diffracting system.

For reducing the level of noise caused by the background fogging and crystal fluorescence, a pair of 0.5 T neodymium-iron-boron permanent magnets, which formed a slit of 10 mm wide, was placed in front of the crystal. Additionally, for registering spectra we used image plate that was not sensitive to the electromagnetic noise. A big advantage of our measurements was using a *high luminosity* focusing spectrometer with spatial resolution (FSSR) (see paper [34] for the details), which allowed increasing dramatically the signal/noise ratio. Indeed, all X-ray spectra intensity emitted by plasma, in the direction perpendicular to the spectra dispersion. was focused in the line with some pxl thickness, so that the signal/noise ratio significantly increased. All the above mentioned arrangements allowed measuring spectra in a single laser shot with a high spectral resolution and a high signal/noise ratio.

Spectra were recorded on Fujifilm TR image plate, which was protected against exposure to visible light using two layers of 1 μm thick polypropylene filter coated with 0.2 μm Al. In addition to these, a 1um thick polypropylene filter was placed at the magnet slit. The spectra were measured from the rear side of the foil: the most intense contribution to the spectral lines originated from the densest part of the plasma, i.e., from the region near the relativistic critical density. It should be emphasized that any spectra of plasma, produced by amplified spontaneous emission (ASE) at the electron density lower than the non-relativistic critical density ($< 10^{21}$ W/cm^2) have not been observed by both front and rear side spectrometers – see for details the experimental results from paper [37] obtained in the same experimental conditions. It is worth emphasizing that the experimental spectra of Si XIV, exhibited in the

Optics EXPRESS

present paper, were observed from the rear side of target, what suggests that no influence of the ASE plasma emission should be important.

Figure 1(b) shows the experimental spectra of Si XIV Ly_β and Ly_γ lines in shots 72 (2μm Si foil) and 89 (1μm Si foil), which were obtained in a single laser shot with duration of 0.6 ps and laser intensities at the surface of the target theoretically estimated as $1.01\text{x}10^{21}$ W/cm^2 and $0.24\text{x}10^{21}$ W/cm^2, respectively. The positions of the dips/depressions in the profiles are marked in insets by vertical lines separated either by $2\lambda_{pe}$ or $4\lambda_{pe}$, where $\lambda_{pe} = \left[\lambda_0^2/(2\pi c)\right]\omega_{pe}$ (λ_0 is the unperturbed wavelength of the corresponding line).

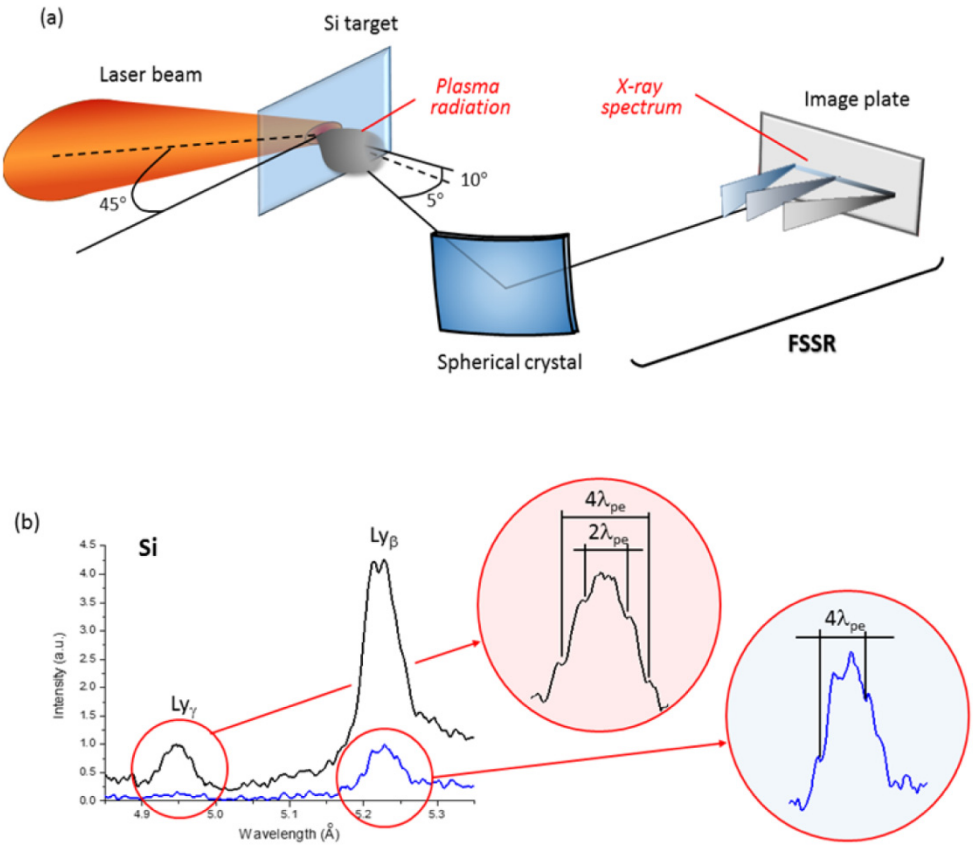

Fig. 1. Schematic of experimental setup and typical X-ray spectra in the range of 0.485 – 0.535 nm. Experimental setup (a) and profiles (b) of Si XIV spectral lines, obtained in a single laser shot with initial laser intensity at the surface of the target estimated as $1.01\text{x}10^{21}$ W/cm^2 (black trace) and $0.24\text{x}10^{21}$ W/cm^2 (blue trace). In the insets, positions of the dips/depressions in the profiles are marked by vertical lines separated either by $2\lambda_{pe}$ or $4\lambda_{pe}$, where $\lambda_{pe} = [\lambda_0^2/(2\pi c)]\omega_{pe}$ (λ_0 is the unperturbed wavelength of the corresponding line).

2.2 Brief theory of Langmuir-wave-caused dips in spectral line profiles

Dips/depressions at specific locations within profiles of hydrogenic spectral lines are typical for plasmas in which Langmuir waves have developed. There is a rich physics behind the phenomenon of the Langmuir-wave-caused dips (L-dips). They result from a resonance between the Stark splitting $\omega_F = 3n\hbar F/(2Z_r m_e e)$ of hydrogenic energy levels, caused by a quasistatic field **F** in a plasma, and the frequency ω_L of the Langmuir wave, which practically coincides with the plasma electron frequency $\omega_{pe}(N_e)$: $\omega_F = s\omega_{pe}(N_e)$ s = 1, 2, … . Here n and Z_r are the principal quantum number and the nuclear charge of the radiating hydrogenic

Optics EXPRESS

atom/ion (radiator). Even for the most common case of $s = 1$, it is actually a multi-frequency resonance phenomenon despite the electric field of the Langmuir wave is considered to be single-frequency (monochromatic): $\mathbf{E}_0 \cos\omega_{pe}t$. This was shown in paper [38]: it is a resonance between many quasienergy harmonics of the combined system "radiator + oscillatory field" caused simultaneously by all harmonics of the total electric field $\mathbf{E}(t) = \mathbf{F} + \mathbf{E}_0 \cos\omega_{pe}t$, where vectors $\mathbf{F}$ and $\mathbf{E}_0$ are not collinear. The quasistatic field $\mathbf{F}$ represents the low-frequency part of the ion microfield and the LET, if the latter was developed in the plasma.

The resonance condition $\omega_F = s\,\omega_{pe}(N_e)$, translates into specific locations of L-dips in spectral line profiles depending on N_e. In particular, for the Ly-lines, in the case where the quasistatic field $\mathbf{F}$ is dominated by the LET, the distance of an L-dip from the unperturbed wavelength λ_0 is given by $\Delta\lambda_{dip}(q,N_e) = -\left[\lambda_0^2/(2\pi c)\right] qs\omega_{pe}(N_e)$. Here $q = n_1 - n_2$ is the electric quantum number expressed via the parabolic quantum numbers n_1 and n_2: $q = 0, \pm 1, \pm 2, \ldots, \pm(n-1)$. It labels Stark components of Ly-lines. For a pair of Stark components, corresponding to q and $-q$, there could be a pair of L-dips located symmetrically in the red and blue parts of the profile: $\Delta\lambda_{dip}(N_e) = \pm\left[\lambda_0^2/(2\pi c)\right] qs\omega_{pe}(N_e)$ for the typical case of the one quantum resonance ($s = 1$). For the two quantum resonance ($s = 2$), in the profile of the same pair of Stark components, there could be another pair of L-dips located symmetrically in the red and blue parts of the profile: $\Delta\lambda_{dip}(N_e) = \pm\left[\lambda_0^2/(2\pi c)\right] q\omega_{pe}(N_e)$.

If the quasi-static field $\mathbf{F}$ is dominated by the ion microfield, then the above formula for $\Delta\lambda_{dip}$ would hold only for relatively low electron densities. For relatively high electron densities, the special non-uniformity of the ion microfield has to be taken into account leading to the result [8,9]

$$\Delta\lambda_{dip}(q,N_e) = -\frac{\lambda_0^2}{2\pi c}\left\{ qs\omega_{pe} + \left[\frac{2\left(s\omega_{pe}\right)^3}{27n^3 Z_r Z_p \omega_{at}}\right]^{1/2}\left[n^2\left(n^2 - 6q^2 - 1\right) + 12n^2q^2\right]\right\}, \quad (1)$$

where Z_p is the charge of the perturbing ions and $\omega_{at} = m_e e^4/\hbar^3 = 4.14\cdot 10^{16}\,s^{-1}$ is the atomic unit of frequency. The first, primary term in braces reflects the dipole interaction with the ion microfield. The second, smaller term in braces takes into account – via the quadrupole interaction – a spatial non-uniformity of the ion microfield. It results in the shift of the midpoint between the pair of L-dips, corresponding to q and $-q$, with respect to the unperturbed wavelength.

In any case (whether the field $\mathbf{F}$ is dominated by the ion microfield or by a LET), the separation of the two L-dips, corresponding to q and $-q$, is

$$\Delta\lambda_{dip}(-|q|,N_e) - \Delta\lambda_{dip}(|q|,N_e) = \left[\lambda_0^2/(\pi c)\right]|q|s\omega_{pe}(N_e), \quad (2)$$

thus allowing to measure N_e. It is important to emphasize that *this passive spectroscopic method for measuring N_e is just as accurate as the active spectroscopic method (more complicated experimentally) using the Thompson scattering*, as shown in the benchmark experiment [8]. The half-width of the L-dip (i.e., the separation between the dip and the nearest "bump"), is controlled by the amplitude E_0 of the Langmuir wave [9]:

$$\delta\lambda_{1/2} \approx \left(\frac{3}{2}\right)^{1/2}\frac{\lambda_0^2 n^2 E_0}{8\pi m_e e c Z_r} \quad (3)$$

Optics EXPRESS

Thus, by measuring the experimental half-width of L-dips, one can determine the amplitude E_0 of the Langmuir wave.

Before analyzing the experimental Si XIV spectral lines, we should note the following. The laser frequency ω corresponds to the wavelength λ of approximately 1054 nm. At lower, non-relativistic laser intensities, the critical electron density N_c determined from the equation $\omega = \omega_{pe}$, where $\omega_{pe} = \left(4\pi e^2 N_e / m_e\right)^{1/2}$, i.e., $\omega_{pe} = \left(4\pi e^2 N_e / m_e\right)^{1/2}$, would be 1.0x10^{21} cm^{-3}. However, at the laser intensities ~10^{21} W/cm^2, i.e. those corresponding to the experiment, due to relativistic effects, the "relativistic" critical electron density N_{cr} becomes higher than N_c [39–41]. For the linearly-polarized laser radiation, it becomes [42]

$$N_{cr} = \frac{(\pi a/4) m_e \omega^2}{4\pi e^2}, \qquad a = \lambda(\mu m)\left[\frac{I\left(W/cm^2\right)}{1.37x10^{18}}\right]^{1/2} \tag{4}$$

The ability of the ultra-intense laser radiation to penetrate into regions of the density higher than

N_c, i.e. a relativistically-induced transparency regime, has been previously demonstrated by PIC simulations [43]. In the present paper we not only took into account the effect of the relativistically induced transparency (details of which can be found in paper [44]) on the resonance condition, but also confirmed that the L-dips originate from the region of the relativistic critical density (which is greater than the nonrelativistic critical density), as shown in the next section.

2.3 Analysis of the experimental spectra and comparison with simulated spectral line shapes

Let us consider the experimental profile of Si XIV Ly-gamma, produced in an interaction with a single laser pulse with initial laser intensity at the surface of the target estimated as 1.01x10^{21} (black trace in Fig. 2(b)). The experimental profile shows a pair of two L-dips nearest to the line center (q = ± 1, s = 1) separated from each other by 28 mÅ yielding an electron density of N_e = 3.6x10^{22} cm^{-3}. In addition to this, a pair of L-dips, separated from each other by 56 mÅ, were also observed, representing a superposition of two pairs of the L-dips: q = ± 2, s = 1 and q = ± 1, s = 2. This yields the same N_e = 3.6x10^{22} cm^{-3}, thus reinforcing the interpretation of the experimental dips as the L-dips – caused by the resonant interaction of the Langmuir waves, developed at the surface of the relativistic critical density, with the quasistatic electric field.

In both cases, L-dips separated by 28 mÅ and for the L-dips separated by 56 mÅ, the mid-point between the two dips in the pair practically coincides with the unperturbed wavelength λ_0. This is a strong indication that the quasistatic field **F** was dominated by the LET. If the LET would be absent, then according to Eq. (1), the mid-point of the pair of the L-dips separated by 28 mÅ should have been shifted by 5.8 mÅ to the red with respect to λ_0 and the mid-point of the pair of the L-dips separated by 56 mÅ would have been similarly shifted by 10.7 mÅ to the red with respect to λ_0, these shifts being due to the spatial non- uniformity of the ion microfield reflected by the 2nd term in Eq. (1).

Another strong indication of the presence of the LET observed from the above result comes from the analysis of the broadening of this spectral line that was performed using code FLYCHK [45]. This code, which does not take into account the Stark broadening by the LET (or the presence of L-dips), yielded N_e = 0.9x10^{23} cm^{-3}, i.e., almost three times higher than the actual N_e = 3.6x10^{22} cm^{-3} (the best fit to the experimental profile by code FLYCHK is shown in Fig. 2(a). This is yet another strong indication of an additional Stark broadening by the LET (not accounted for by FLYCHK).

Optics EXPRESS

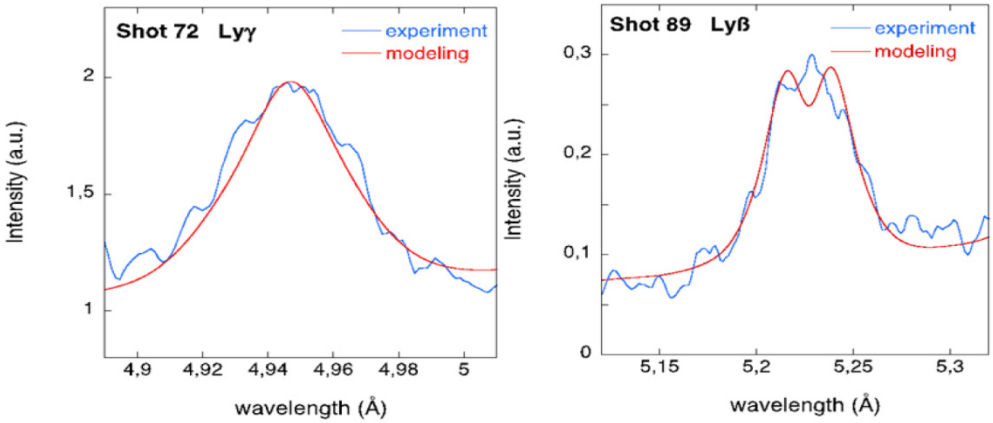

Fig. 2. Experimental spectra and their comparisons with FLYCHK modeling. (a) Comparison of the experimental profile of Si XIV Ly_γ line in shot with initial laser intensity at the surface of the target estimated as 1.01×10^{21} W/cm^2 with a simulation performed using a variation of the code FLYCHK for calculating the Stark broadening, then adding both Doppler and instrument broadening, and, if necessary, opacity. The L-dips phenomenon and the spectral line broadening by LET were not included in the FLYCHK. The plasma parameters for the best fit are $N_e = 0.9 \times 10^{23}$ cm^{-3} and $T_e = 500$ eV. b) The same as in (a) but for Si XIV Ly_β line produced in a single laser shot with initial laser intensity at the surface of the target estimated as 0.24×10^{21} W/cm^2 ; $N_e = 3 \times 10^{23}$ cm^{-3} and $T_e = 500$ eV.

At the initial laser intensity at the surface of the target estimated as 1.01×10^{21} W/cm^2, the relativistic critical density would be $N_{cr} = 2.3 \times 10^{22}$ cm^{-3} according to Eq. (4). However, due to several physical effects, the actual intensity of the transverse electromagnetic wave in the plasma can be significantly higher than the intensity of the incident laser radiation at the surface of the target. One of these effects is the self-focusing of the laser beam in plasmas - details of the process of the laser propagation in the plasma corona at the overcritical density can be found, for example, in papers [44,46] and in reviews [21,47]). The other effects are Raman and Brillouin backscattering, For example, in paper [48] this was proven by a spectroscopic analysis of the experimental X-ray line profiles and by PIC simulations. In the present experiment in shot 72, for the relativistic critical density to be approximately equal to the density $N_e = 3.6 \times 10^{22}$ cm^{-3} deduced by the spectroscopic analysis, it would require the enhancement of the initially estimated intensity of the transverse electromagnetic wave at the surface of the target due to the above physical effects just by a factor of two.

We also evaluated (independently of the spectroscopic analysis) the enhancement of laser intensity due to the self-focusing from the well-known model – see, e.g., Chap. 4 of book [49]. Taking into account our plasma parameters one can get the enhancement of the laser intensity by the factor of two, which was consistent with the results of our spectroscopic analysis.

Previous studies have shown (see, e.g., [21,22]) that at high laser intensities, the most probable and the best studied mechanism for developing Langmuir waves at the surface of the relativistic critical density is a parametric decay, which is a nonlinear process where the pump wave (t_1) excites both the Langmuir wave (l) and an ion-acoustic wave (s): $t_1 \rightarrow l + s$. In shot 72, we experimentally discovered LET, which developed simultaneously with the Langmuir waves. Therefore, first, the LET should have been also developed at the surface of the relativistic critical density and thus should have been most probably the ion acoustic turbulence. Second, the self-focusing, as well as Raman and Brillouin backscattering most probably enhanced the intensity of the transverse electromagnetic wave in the plasma by a factor of two. To further prove these conclusions we performed also PIC simulations at the electromagnetic wave intensity enhanced by a factor of two. These simulations confirmed the

Optics EXPRESS

development of both Langmuir and ion acoustic waves, as presented in detail in the next section.

We mention in passing that L-dips were not observed in the experimental profiles of Si XIV Ly_α and Ly_β lines in shot 72. It seems that a process of self-absorption of radiation prevented L-dips from being visible in these lines: the self-absorption "washes out" fine features of the experimental profiles.

The analysis of the experimental profile of Si XIV Ly_β in shot 89 with the initial laser intensity at the surface of the target estimated as $2.4\text{x}10^{20}$ W/cm^2 (blue trace in Fig. 1(b)), shows a situation similar to Si XIV Ly_γ in shot 72. There is a pair of the L-dips separated from each other by 43 mA. The electron density deduced from the separation within the pair of these L-dips, is $N_e = 1.74\text{x}10^{22}$ cm^{-3} (assuming $|q|s = 2$ in Eq. (2)). The location of the would-be L-dips, corresponding to $|q|s = 1$, is too close to the central, most intense part of the experimental line profile: they are not observed either due to a self-absorption in the most intense part of the profile, or because the relatively small values of the field F, corresponding to the central part of the profile, are not quasistatic (as it is well-known from review [50]). So, the would-be L-dips, corresponding to $|q|s = 1$ could not form for either or both reasons.

The mid-point between the two dips in the pair practically coincides with the unperturbed wavelength λ_0. This is again a strong indication that the quasistatic field **F** was dominated by the LET. If the LET would be absent, then according to Eq. (1), the mid-point of this pair of the L-dips should have been shifted by 6.1 mÅ to the red with respect to λ_0.

Another strong indication of the presence of the LET in shot 89 comes from the analysis of the broadening of this spectral line is following from the modeling, which was performed using code FLYCHK [45]. An electron density of $N_e = 3\text{x}10^{23}$ cm^{-3}, was obtained, i.e. 17 times higher than the experimentally verified $N_e = 1.74\text{x}10^{22}$ cm^{-3} (the best fit to the experimental profile by code FLYCHK is shown in Fig. 2(b)). This is yet another strong indication of an additional Stark broadening by the LET (not accounted for by FLYCHK).

At the initial laser intensity at the surface of the target estimated as $2.4\text{x}10^{20}$ W/cm^2, the relativistic critical density would be $N_{cr} = 1.1\text{x}10^{22}$ cm^{-3} according to Eq. (4). However, again due to the self-focusing, as well as Raman and Brillouin backscattering, the actual intensity of the transverse electromagnetic wave in the plasma can be significantly higher. In the present experiment in shot 89, for the relativistic critical density to be approximately equal to the density $N_e = 1.74\text{x}10^{22}$ cm^{-3} deduced by the spectroscopic analysis, again it would require the enhancement of the intensity of the transverse electromagnetic wave due to the above physical effects just by a factor of two. By the same reasoning as presented above with regard to shot 72, the experimentally discovered LET in shot 89, which developed simultaneously with the Langmuir waves, should have been also developed at the relativistic critical density surface and thus is most likely to be ion acoustic turbulence.

In shot 89, L-dips were not observed in the experimental profiles of Si XIV Ly_α and Ly_γ lines. This is because the Ly_α line seemed to experience a significant self-absorption, which prevented L-dips from being visible. As for the Ly_γ line in shot 89, at the possible locations of the L-dips, the experimental profile already merged into the noise.

For a further quantitative analysis, we calculated the corresponding theoretical profiles, where the total quasistatic field is $\mathbf{F} = \mathbf{F_t} + \mathbf{F_i}$. For calculating the distributions of the total quasistatic field $\mathbf{F} = \mathbf{F_t} + \mathbf{F_i}$, where $\mathbf{F}_t$ is the field of a LET and $\mathbf{F}_i$ is the quasistatic part of the ion microfield, we employed the results from references [51,52]: the distribution of the total quasistatic field is a convolution of the Rayleigh-type distribution of F_t [51] with the APEX distribution of F_i [53]. The broadening by the electron microfield, as well as the Doppler and instrumental broadenings were also taken into account. For calculating the spectra in the regions of L-dips we used the analytical solution [9,38] for the wave functions of the quasienergy states caused simultaneously by all harmonics of the total electric field $\mathbf{E}(t) = \mathbf{F} + \mathbf{E}_0 \cos\omega_{pe}t$, where vectors **F** and $\mathbf{E}_0$ are not collinear. Further details can be found in paper [38] and in book [9], Sect. 4.2. Below is the outcome.

Optics EXPRESS

From the experimental profile of Si XIV Ly-gamma in shot 72, it follows that the root-mean-square value of F_t was $F_{t,rms}$ = 2.1 GV/cm. For comparison, the characteristic ion microfield $F_{i,typ} = 2.603\ eZ^{1/3}N_e^{2/3}$ was 1.0 GV/cm. From the half width of the experimental L-dips, by using Eq. (3), we found the amplitude of the Langmuir wave to be E_0 = 0.6 GV/cm. The resonant value of the quasistatic field F_{res}, determined by the condition of the resonance between the separation of the Stark sublevels and the plasma frequency $3n\hbar F_{res}/(2Z_r m_e e) = \omega_{pe}$, was 3.1 GV/cm, so that the validity condition for the existence of L-dips $E_0 < F_{res}$ [9] was satisfied.

From the experimental profile of Si XIV Ly-beta in shot 89, it follows that the root-mean-square value of F_t was $F_{t,rms}$ = 3.9 GV/cm. For comparison, the characteristic ion microfield was $F_{i,typ}$ = 0.6 GV/cm. From the halfwidth of the experimental L-dips, by using Eq. (3), we found the amplitude of the Langmuir wave to be E_0 = 1.0 GV/cm. The resonant value of the quasistatic field was F_{res} = 5.8 GV/cm, so that the validity condition for the existence of L-dips $E_0 < F_{res}$ was satisfied.

The comparison of the theoretical profiles, allowing, in particular, for a LET and L-dips, with the corresponding experimental profiles is shown in Fig. 3.

The good agreement between experimental spectra and simulations reinforces the discovery of the simultaneous production of LET with the Langmuir waves. We note that the electron densities involved turned out to be much lower than the densities deduced using FLYCHK simulations, which ignored the LET and the L-dips.

One more point should be clarified. A Langmuir wave $\mathbf{E}_0\ cos\omega_p t$, considered without the presence of a quasistatic field **F** in plasmas, could produce satellites [54], which for the Ly lines would be at the same locations as the L-dips. However, it had been shown analytically (Sect. 7.3 of book [9]) that at the presence of the quasistatic field in plasmas, the local "zigzag" of the intensity due to the L-dip is much stronger than the local "zigzag" of intensity due to a would-be satellite at the same location in the spectral line profile. Therefore, Langmuir waves in plasmas always manifest as L-dips rather than satellites.

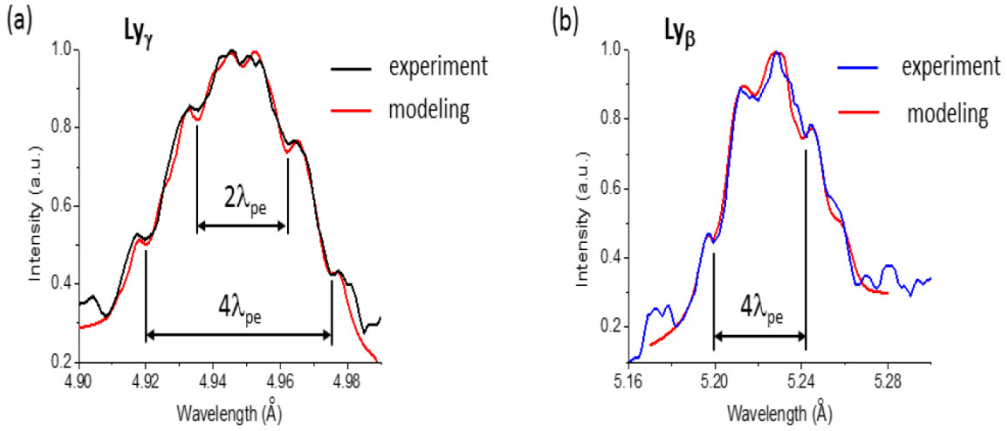

Fig. 3. Experimental spectra and their comparisons with a different Stark broadening code including L-dips and the spectral line broadening by LET. a) Experimental spectra of Si XIV Ly_γ line in a single laser shot with initial laser intensity at the surface of the target estimated as 1.01×10^{21} W/cm^2 initial laser intensity at the surface of the target. The positions of the dips/depressions in the profiles are marked by vertical lines separated either by $2\lambda_{pe}$ or $4\lambda_{pe}$, where $\lambda_{pe} = [\lambda_0^2/(2\pi c)]\omega_{pe}$ (λ_0 is the unperturbed wavelength of the corresponding line). Also shown is a theoretical profiles at $N_e = 3.6\times10^{22}$ cm^{-3} allowing, in particular, for a low-frequency electrostatic turbulence (see the text for details). b) Same but for Si XIV Ly_β line in a single laser shot with initial laser intensity at the surface of the target estimated as 0.24×10^{21} W/cm^2 initial laser intensity at the surface of the target. The theoretical profile is shown at $N_e = 1.74\times10^{22}$ cm^{-3}.

Optics EXPRESS

We also performed experiments where the spectrometer viewed the laser-irradiated *front* surface of the target. As an example, Fig. 4 shows the experimental spectrum of Al XIII Ly_β line in shots 82 (4 μm Al foil coated by 0.45 μm CH), which was obtained in a single laser shot with duration of 0.9 ps and the laser intensity at the surface of the target theoretically estimated as $6.7x10^{20}$ W/cm^2.

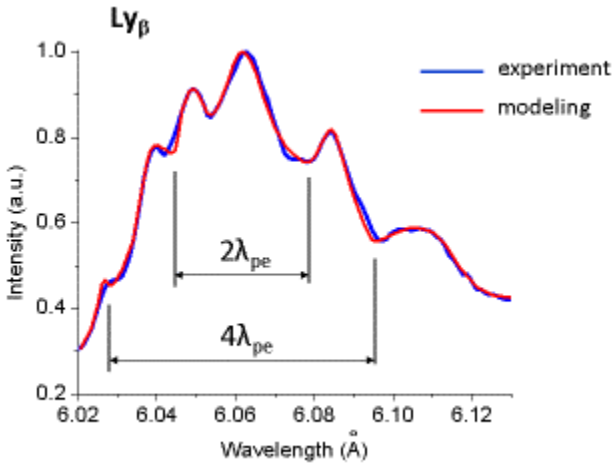

Fig. 4. Experimental spectrum of Al XIII Ly_β and its comparison with the Stark broadening code including L-dips and the spectral line broadening by LET. The experimental spectrum was obtained in a single laser shot with initial laser intensity at the surface of the target estimated as $6.7x10^{20}$ W/cm^2. The positions of the L-dips in the profiles (the L-dips being very pronounced) are marked by vertical lines separated either by $2\lambda_{pe}$ or $4\lambda_{pe}$, where $\lambda_{pe} = [\lambda_0^2/(2\pi c)]\omega_{pe}$ (λ_0 is the unperturbed wavelength of the corresponding line). Also shown is a theoretical profile at $N_e = 2.35x10^{22}$ cm^{-3} allowing, in particular, for L-dips and for a low-frequency electrostatic turbulence. This value of N_e is much lower than N_e obtained from fitting the same experimental spectrum by code FLYCHK that did not include the L-dips phenomenon and the spectral line broadening by LET, and therefore had significant discrepancies with the experimental profile at the locations of the L-dips.

This spectrum exhibits two pairs of L-dips: one pair – at ± 16.8 mA from the line center, another pair – at ± 33.6 mA from the line center. The L-dips are very pronounced: for example, for the L-dips at ± 16.8 mA from the line center, the intensity of the bump nearest to the center of the dip exceeds the intensity at the center of the dip by 15% for the L-dip at + 16.8 mA and by 11% for the L-dip at –16.8 mA. Just by itself, such a strong modulation of the line profile clearly indicates that it is not a noise. More importantly – and this argument concerns all of the above spectra – the fact that the observed dips are located *symmetrically* (rather than randomly) with respect to the line center (located at 6.06 A) indicates that this is not a noise. This is especially clear in cases where two pairs of symmetrically-located L-dips were observed (such as in Al XIII Ly_β spectrum in shot 82 and in Si XIV Ly_γ spectrum in shot 72): not only there was the symmetry (rather than randomness) in terms of the dips location within each pair, but also the distance from the line center for one pair was consistent (differed exactly by the factor of 2, as theoretically expected) with the distance from the line center for the second pair.

Finally we note that the characteristic lifetime of the upper state n of the radiating ion (i.e., of the state, from which the observed spectral line originates), being controlled by the electron dynamical broadening, is much smaller than the period of the LET. Therefore, each radiating ion "transmits" to the spectrometer a snapshot of the instantaneous electric field of the LET at the location of the radiating atom. This is the essence and the justification of the quasistatic description of the LET. Different radiating ions are subjected to different values of the LET

fieldstrength, so that the averaging/integration over the ensemble of the radiating ions conveys the distribution of the electric field of the LET. Since the radiating ions are constantly excited to the upper state n (followed by the decay) at various times during the laser pulse and at various locations, there are always radiating ions that "witness" the LET resulting from the development of the parametric decay instability.

Also it should be emphasized that measurements of plasma parameters by intensity ratios of various lines of H and He-like ions of Si, processed for the same experimental conditions by Los Alamos code Atomic [37], clearly demonstrated that the plasma emission originated from the region of the electron density of about 10^{22} W/cm^2 . Those results are in a good agreement with the results of the present paper, the latter including the influence of the parametric instabilities on the X-ray spectra.

Figure 5 presents a sketch of the interlinked physical processes from atomic/optical physics and plasma physics relevant to the present paper and showing that laser-plasma interaction phenomena can be revealed through atomic/optical physics diagnostics.

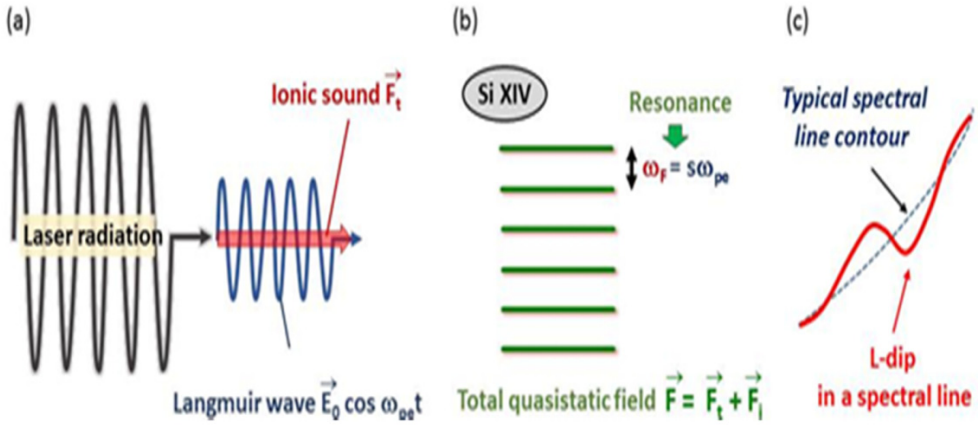

Fig. 5. Sketch of the interlinked physical processes from plasma physics and atomic physics relevant to the present paper. a) Parametric decay of the laser radiation into a Langmuir wave and an ion acoustic wave at the surface of the relativistic critical density. b) Resonance between the Stark splitting ω_F of the levels of Si XIV in the total quasistatic field (**F**), which is dominated by the field $(\mathbf{F})_t$ of the ion acoustic wave, with the plasma electron frequency or its harmonics: $s\omega_{pe}$, s = 1,2,.. . c) Magnified part of the experimental profile showing an L-dip resulting from the above resonance (solid line); the dashed line shows the profile at the absence of the above Langmuir waves in the plasma.

2.4. PIC simulations

The results of our spectroscopic analysis have been also supported by PIC simulations. The simulations were performed using the modified 1D PIC code LPIC, in which a laser pulse of duration t_L = 0.6ps and intensity I_L = 2.7x10^{21} W/cm^2 interacted with a Si [55]. Laser pulse propagates along the x-axis and interacts with Si^{+14} inhomogeneous plasma layer with a linear density ramp over the length L = 6 μm and a target thickness of 2um, with a constant ion density of N_i = 6x10^{22} cm^{-3}. Angle of incidence was set up 45° at P – polarization. The results of the simulations are shown in Fig. 6.

At the peak of the laser pulse intensity (t = 320 fs) it is seen that the scale of laser field decay is close to the scale of the plasma inhomogeneity. The longitudinal field of the Langmuir wave E_l appeared in the vicinity of the point where the density is about 1/4 of the relativistic critical density. The Langmuir wave exists up to a point slightly above the relativistic critical density N_{cr} = 3.6x10^{22}cm^{-3}. In Fig. 5(b), the region near the relativistic critical density is $8\lambda < x < 8.25\lambda$: the modulation of ion density in this region shown by the green line is the manifestation of the ion acoustic wave. Similar processes of such parametric

Optics EXPRESS

decays ($t \rightarrow l + l', s$) were studied in the past (see, e.g., book [56]), but for significantly lower laser intensities.

3. Summary

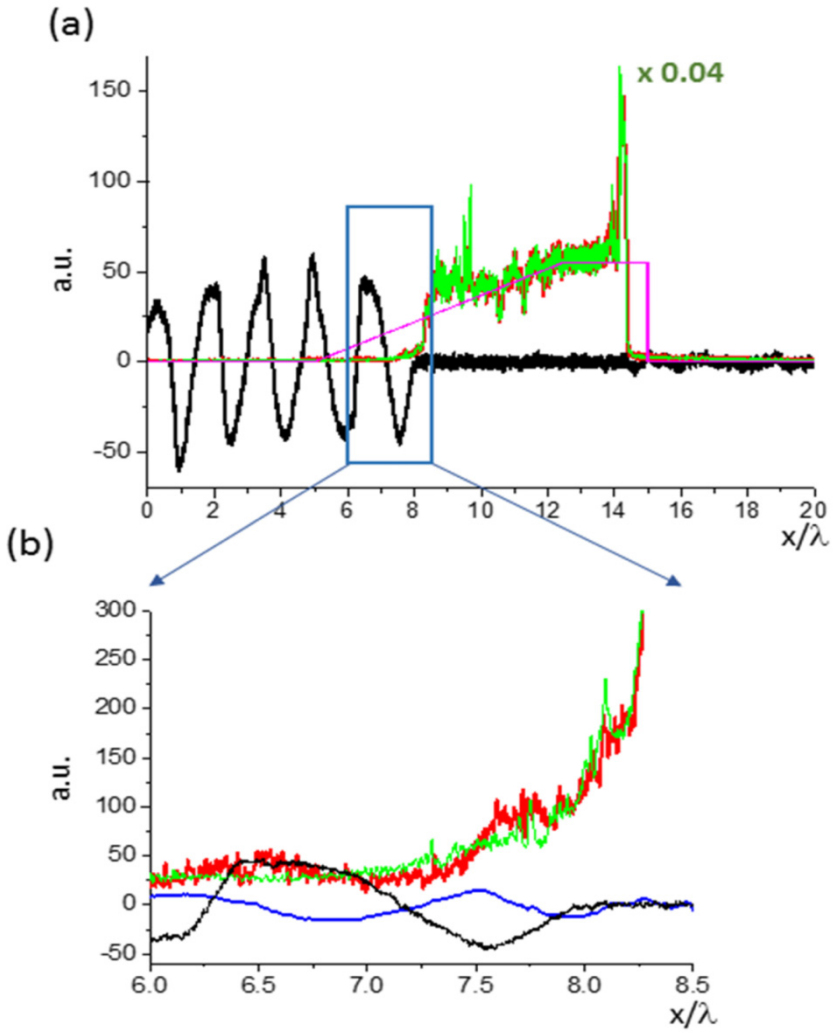

Fig. 6. PIC simulations of the interaction of a 600 fs pulse of the intense (2.7×10^{21} W/cm^2) linearly-polarized laser radiation with the Si^{14} plasma layer. The general view of the laser-target interaction at the instant t = 320 fs from the beginning of the interaction (a) and the zoom (b) on the area shown by the black rectangle in (a). The coordinate x is in units of the laser wavelength λ. The initial scaled density profile is presented by the violet line. The scaled electron and ion densities are presented by the red and green lines. They are given in the units of $0.04ZN_{cr}$ in (a) and in the units of ZN_{cr} in (b); here $N_{cr} = \gamma N_c$, where N_c is the critical plasma density and $\gamma = a_L$ is the relativistic factor. The calculated scaled transversal electric field $a_L = eE_L/(m_e\omega_L c)$ is shown by the black line and the longitudinal one (the Langmuir wave) $a_l = eE_l/(m_e\omega_L c)$ – by the blue line.

We analyzed the experimental spectra of Si XIV and Al XIII lines obtained at the interaction of a super-intense laser radiation with thin Si foils. The analysis shows that Langmuir waves developed at the surface of the relativistic critical density. It is well-known that at high laser intensities, the most probable and the best studied mechanism for developing Langmuir waves at the surface of the critical density is the PDI, which is a nonlinear process where the pump

Optics EXPRESS

wave (t_1) excites both the Langmuir wave (l) and an ion-acoustic wave (s): $t_1 \rightarrow l + s$. Therefore, the experimentally discovered LET, which developed simultaneously with the Langmuir waves, will have also been developed at the surface of the critical density and thus will most probably have been the ion acoustic turbulence. These conclusions have been also supported by PIC simulations. We determined both the amplitude of the Langmuir waves and the root-mean-square field of the ion acoustic waves.

The ratio of the energy density of the turbulent electric fields $E^2/(8\pi)$ to the thermal energy density of the plasma N_eT in this experiments was ~10^{-1}. In atmospheres of quasars, pulsars, and Seyfert galaxies, the electron density is at least by 12 orders of magnitude lower than in the above experiments, but the order of magnitude of the ratio $E^2/(8\pi N_eT)$ is a similar to the order of magnitude of this ratio in the above experiments. Since the conditions for developing the PDI are satisfied for atmospheres of these astrophysical objects [28], the above type of laboratory experiments could serve as a tool for modeling the PDI in these astrophysical objects. The principle of modeling astrophysical objects in laboratory experiments based on the similarity of dimensionless controlling parameters was already successfully used, e.g., in laboratory modeling of mechanisms of solar flares (see, e.g., review [29]).

Our spectra were integrated over the pulse duration. Time-resolved X-ray spectroscopy had been already performed for similar experimental situations – see, e.g., paper [44]. In that paper it was shown from the Li-like emission history for Al thin foils that during 700fs the *electron density* of the plasma, deduced from the broadening of the lines, was very high (solid-state density) and *steady*. It was attributed to the hottest plasma produced during the highest laser intensity. After 700fs there was no significant signal that would come from colder plasma. So, we interpreted our experimental results (in this regard) the same way as in paper [44].

The idea of employing these two different codes simultaneously should be applied to other spectroscopic experiments in laser-produced plasmas showing identifiable L-dips. The identification of L-dips in the experimental line profiles provides a very accurate determination of the electron density N_e independent of the broadening of the spectral lines. Then if a code like FLYCHK, ignoring the LET and the L-dips, yields a much higher value of N_e than the one deduced from the L-dips, this would be an indication of the development of the LET in those other experiments.

Thus, our results should be important from both theoretical and practical points of view. The experimental discovery of the ion acoustic turbulence in laser-plasma experiments is an important new result in its own right, enabling the comparison of theoretical predictions concerning the development of the ion acoustic waves with the experimentally determined parameters of these waves. Our results can be also used for important practical purposes, such as: A) modeling physical processes in atmospheres of quasars, pulsars, and Seyfert galaxies – in particular, the PDI, causing the anomalous absorption of the incident electromagnetic radiation; B) providing a better understanding of the physics of laser-produced plasmas, in particular, the transport phenomena (especially, the anomalous resistivity) – as they are strongly affected by the ion acoustic waves.

Funding

RAS Presidium Program for Basic Research Program #13 and Competitiveness Program of NRNU MEPhI.

Acknowledgements

We thank the Vulcan technical and target preparation teams at the Central Laser Facility for their support during the experiments.